Structural, hyperfine, and magnetic properties of R_2FeTaO_7 compounds (R=Y, Dy, Gd, and Eu)

C. Kimie Matsuda,[1] F. F. Ivashita,[1] A Paesano, Jr.,[1] E. V. Pannunzio Miner,[2] M. C. Blanco,[2] R. E. Carbonio,[2] J. B. Marimon da Cunha,[3] and L. Ghivelder[4]
[1]*Departamento de Física, UEM, Av. Colombo, 5790 87.020-900 Maringá, PR, Brazil*
[2]*INFIQC-CONICET, Depto. de Físico-Química, Universidad Nacional de Cordoba, Argentina*
[3]*Instituto de Física, UFRGS, Porto Alegre, RS, Brazil*
[4]*Instituto de Física, UFRJ, Rio De Janeiro, RJ, Brazil*
(Received 26 June 2009; revised manuscript received 23 October 2009; published 22 January 2010)

Pyrochlore-related compounds of the R_2FeTaO_7 type (with R=Gd, Eu, Dy, and Y) were synthesized by solid-state reaction of precursor oxides. The compounds were structurally and magnetically characterized by x-ray diffraction, Mössbauer spectroscopy, and magnetic measurements. The results revealed that this subfamily of pyrochlores crystallizes with the $\mathbf{R\bar{3}}$ symmetry, where iron with tantalum occupies two different crystallographic sites. Magnetic phase transition to a long-range ordered state was not observed down to 2 K, although islands of magnetically oriented iron atoms could be detected.

DOI: 10.1103/PhysRevB.81.014417 PACS number(s): 75.50.−y

I. INTRODUCTION

Pyrochlores are oxides with the ideal formula $A_2B_2O_7$, where A and B are in general trivalent and tetravalent cations, respectively. These compounds are predominantly cubic and ionic in nature, and represent a family of phases that are isostructural to the mineral pyrochlore (NaCa)(NbTa)O_6F/(OH). The $A_2B_2O_7$ compounds exhibit a wide variety of interesting physical properties, the geometric magnetic frustration being the most striking.[1–3]

It is possible to synthesize these compounds with different chemical elements at the A or B sites, provided that the ionic radius and charge neutrality criteria are satisfied.[4,5] For the most of the pyrochlores studied in the phenomenology scenario of magnetic frustration, A is a magnetic rare-earth element (R) and B is a nonmagnetic metal (e.g., Ti, Sn, and Zr). In these cases, the only magnetic sublattice is the one made by the rare-earth cations, which form a structure of sharing corners tetrahedral. Thus, one may speculate if the introduction of a magnetic cation (e.g., Mn, Cr, or Fe) in B sites could affect or, even, raise the degeneracy of the magnetically frustrated state.

In this sense, only a few iron-containing pyrochlores (ICP) of the $A_2(Fe,B)O_7$ type, where B is a pentavalent or hexavalent cation (transition metal or semimetal) and A is a R, have been previously synthesized. To the best of our knowledge, only the R_2FeSbO_7,[6–9] R_2FeMoO_7,[10] and $Y_2Fe_{1.33}W_{0.67}O_7$ (Ref. 11) compounds have been prepared and characterized to date, in spite of their potentially interesting properties. Aiming to extend the investigation of this class of compounds, we have successfully prepared several ICP and characterized them by x-ray diffraction, magnetization techniques, and Mössbauer spectroscopy.

Mössbauer spectroscopy is a useful technique to analyze these compounds since the nuclear probe ^{57}Fe is present in their structure. However, it has seldom been applied to study this interesting class of oxides, principally regarding low-temperature studies. Indeed, among the previously synthesized ICP's, some choices for the B atom have not been Mössbauer characterized yet, even at room temperature (RT).

In previous studies, x-ray diffraction results revealed that the R_2FeSbO_7 pyrochlores have the same cubic structure as the ternary pyrochlores $\mathbf{Fd\bar{3}m}$,[6–9] although the R_2FeMoO_7 family was shown to be rhombohedral or monoclinic.[10,11] In addition, the onset of magnetic order was observed through the magnetic splitting of the R_2FeSbO_7 (Refs. 6, 8, and 9) and $Y_2Fe_{1.33}W_{0.67}O_7$ (Ref. 11) Mössbauer spectra.

In this paper, a detailed investigation of some R_2FeTaO_7 phases is reported. By combining Rietveld, Mössbauer and magnetic analyses, the structural and magnetic properties of these pyrochlore-related compounds were determined.

II. EXPERIMENTAL DETAILS

The R_2FeTaO_7 (with R=Y, Gd, Eu, and Dy) samples were prepared, first, by ball milling a blend of R_2O_3, Fe_2O_3 and Ta_2O_5 powders (99.9% pure), mixed in a 2: 1: 1 molar ratio. The precursors were milled for 3 h in a vial of alumina (80 ml) with zirconia rods, under argon atmosphere, using a planetary ball mill. The ball-to-powder mass ratio was 20:1 and the rotation speed was 300 rpm. After milling, the powders were annealed under oxygen atmosphere for 24 h, in the 1200–1400 °C temperature range. The samples were cooled to room temperature in the turned off furnace.

The compounds were structurally and magnetically characterized by powder x-ray diffraction, Mössbauer spectroscopy (MS) and magnetic measurements. The x-ray diffractograms were measured using the Cu $K\alpha$ radiation in a conventional diffractometer, in θ-2θ Bragg-Brentano geometry. The 2θ range was from 10° up to 120° with increments of 0.02° and a counting time of 2 s per step. The FULLPROF code[12] was used to refine the crystal structure by the Rietveld method. A pseudo-Voigt shape function was used to fit the experimental data. Refined data were atomic positions, background, lattice, peak shape, and thermal isotropic parameters.

Mössbauer spectra were taken from a constant acceleration spectrometer with a $^{57}Co(Rh)$ source using absorbers with nearly 67 mg/cm^2. For the low-temperature Mössbauer measurement, a helium flow cryostat was used. Magnetic measurements of randomly pressed powders were performed

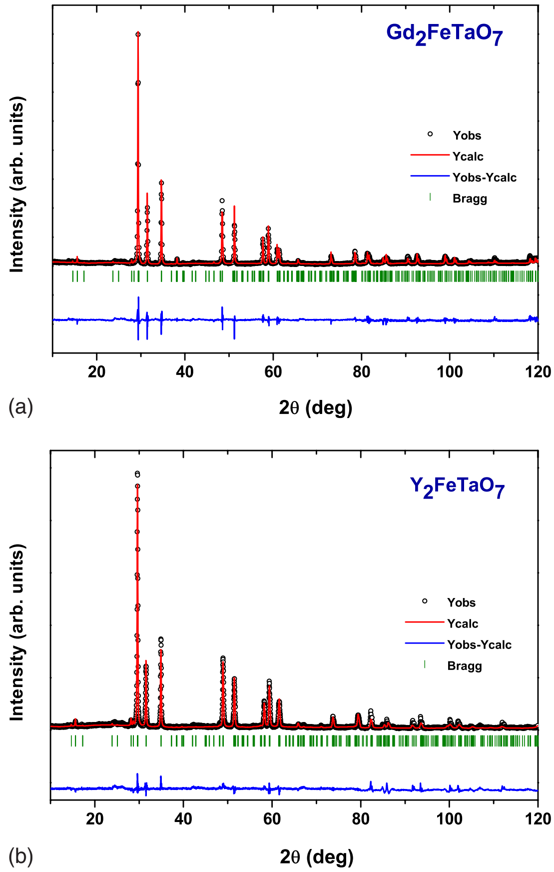

FIG. 1. (Color online) X-ray diffractograms for the (a) Gd_2FeTaO_7 and (b) Y_2FeTaO_7 samples.

in an extraction magnetometer (Quantum Design—Physical Properties Measurement System/PPMS), at temperatures down to 2 K and applied magnetic field up to 9 T.

III. RESULTS AND DISCUSSIONS

The powder diffractograms obtained for the Gd_2FeTaO_7 and Y_2FeTaO_7 compounds are shown in Fig. 1. Apart from small variations in the peaks position and intensity, reflecting the expected variations in the lattice parameters and scattering factors, both compounds revealed the same crystallographic structure, although different from that of ternary pyrochlores (with the **Fd$\bar{3}$m** symmetry). The Rietveld refinement of the diffractograms for all samples revealed that the compounds crystallized in the **R$\bar{3}$** symmetry, and the hexagonal unit cell with lattice parameters of approximately $\sqrt{2}a_f$ ($\approx$7.5 Å) and $2\sqrt{3}a_f$ ($\approx$17 Å), respectively, for a and c, where a_f is the lattice parameter of the parent cubic fluorite cell. Therefore, this is different from what happens when antimony is the partner of iron.[7] Table I shows some Rietveld refined parameters for all prepared samples.

For this particular space group, there are two Wyckoff sites for the R ions (sites $3b$ and $9d$) and two for the transitions metals (sites $3a$ and $9e$).[13] The iron or tantalum atoms from both sites form planes and are surrounded by six or eight oxygen atoms, forming distorted octahedra (site $9e$) and distorted square antiprisms (site $3a$), respectively, as shown in Fig. 2 for the Gd_2FeTaO_7 compound. In this structure, there is a kagome bidimensional net formed by $9e$ sites and a triangular lattice formed by the $3a$ sites which fills in the kagome lattice making a smaller triangular lattice. The rare-earth lattice is the same as the iron-tantalum lattice but shifted by 001/2. Interestingly, the distance between these R basal planes (5.78 Å for Gd_2FeTaO_7) are larger than those equivalent in the ordinary structure [i.e., the planes (111), separated by 4.2 Å, for $Gd_2Ti_2O_7$].

It is worthy of note that the volume of the unit cell showed to increase according to the series Y$<$Dy$<$Gd$<$Eu, which is consistent with the ionic radii variation due to the lanthanide contraction, in addition to the fact that yttrium is smaller in size than the present R's. Figure 3 shows the RT Mössbauer spectra for the same earlier samples. The fitted hyperfine parameters for these and all other compounds, including the values obtained at low temperatures (see spectra ahead), are listed in Table II.

Both RT spectra present two doublets and resemble those our results obtained for the R_2FeNbO_7 compounds.[6] Since the subspectral area of the $3a$ site cannot surpass 0.5 (with the assumption of equal f factors for both sites), it is inferred

TABLE I. Crystallographic refined parameters, as obtained from the Rietveld analysis, for the R_2FeTaO_7 samples.

Pyrochlore ⇒	Y_2FeTaO_7	Dy_2FeTaO_7	Gd_2FeTaO_7	Eu_2FeTaO_7
Cell parameters (Å)				
a	7.4428(2)	7.4680(2)	7.5159(4)	7.5428(3)
c	17.0043(3)	17.0063(2)	17.0609(1)	17.0864(1)
Site occupancies (Fe/Ta)				
($3a$)	0.23(1)/0.27(1)	0.25(1)/0.25(1)	0.33(1)/0.17(1)	0.28(1)/0.22(1)
($9e$)	0.77(1)/0.73(1)	0.75(1)/0.75(1)	0.67(1)/0.83(1)	0.72(1)/0.78(1)
Oxygen atomic coordinates				
O1	0.337(3) 0.171(4) 0.780(2)	0.327(1) 0.158(3) 0.778(2)	0.331(6) 0.204(1) 0.773(8)	0.327(2) 0.163(3) 0.776(5)
O2	0.665(3) 0.793(3) 0.980(9)	0.660(2) 0.783(4) 0.977(3)	0.745(4) 0.871(7) 0.979(5)	0.682(6) 0.801(2) 0.981(7)
O3	0 0 0.9097(3)	0 0 0.932(7)	0 0 0.901(7)	0 0 0.934(5)
R_{wp}	13.0	12.1	13.0	12.9
χ^2	2.90	2.82	3.04	2.87

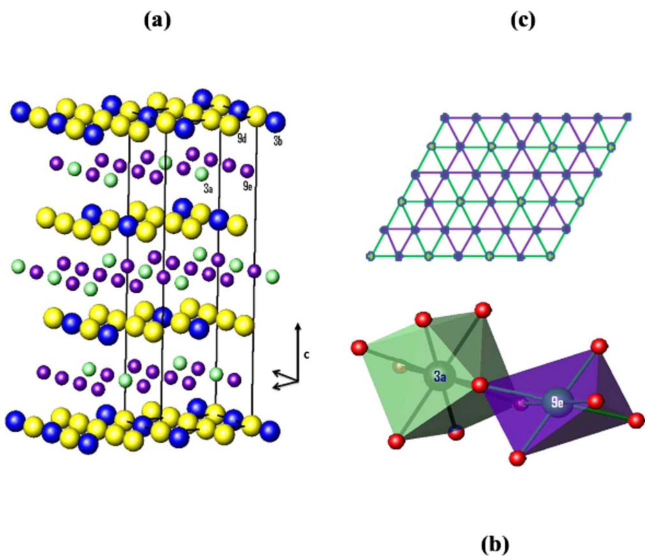

FIG. 2. (Color online) (a) Unit cell for the Gd_2FeTaO_7 compound, showing R layers (yellow and blue balls) alternately stacked between iron (tantalum) layers (green and violet balls), parallel to the (001) plane; (b) octahedral and dodecahedral iron sites in the $\mathbf{R\overline{3}}$ structure—oxygens are in red; (c) iron (tantalum) bidimensional lattice, showing the kagome net and the triangular array formed by the $9e$ (violet) and $3a$ (green) iron atoms, respectively.

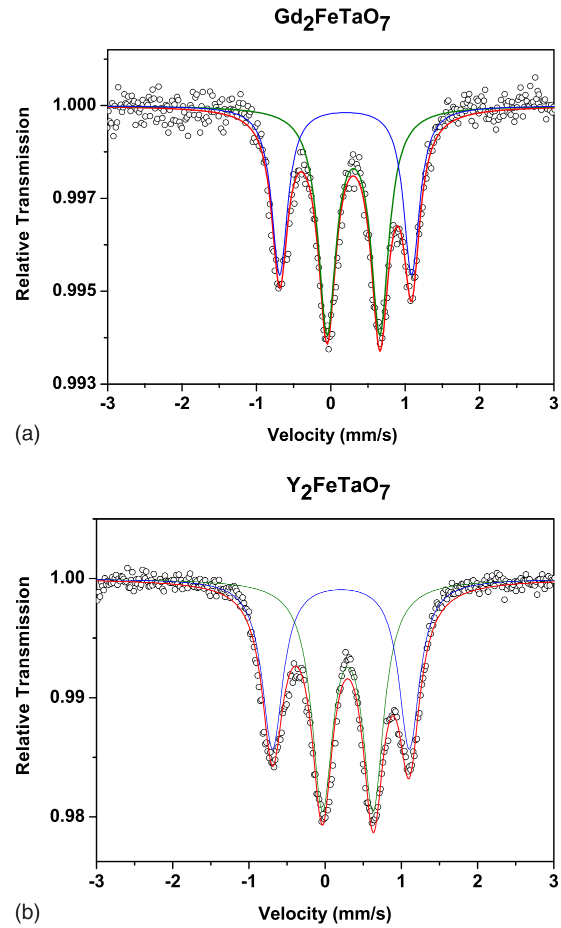

FIG. 3. (Color online) RT Mössbauer spectra for the (a) Gd_2FeTaO_7 and (b) Y_2FeTaO_7 samples.

that the—nearly 150%—larger doublet belongs to the site $3a$ whereas the smaller doublet is relative to the site $9e$.

However, in spite of the experimental evidence, a calculation for the elements of the diagonal electric field gradient (EFG), V_{ii}'s, based on the point-charge approximation[14] and considering only the nearest neighbors (i.e., the oxygen anions), showed that site $3a$ should have only a 35% larger quadrupolar interaction than the site $9e$ (see Table III). In the table, ζ is the angle between the principal Z axis and the crystallographic c axis, as obtained from the diagonalized EFG tensor. Actually, either the octahedra (sites $9e$) or the square antiprisms (sites $3a$) present three different orientations around the crystallographic c axis, although all of them with the same zenithal angle because of the threefold symmetry of this axis.

On the other hand, the isomer shifts for the $3a$ iron sites are displaced from the ordinary range of ferric cations toward lower values (i.e., $IS_{AVE} \approx 0.20$ mm/s). This means that iron was oxidized beyond the trivalent state, eventually to a $Fe^{3+,4+}$ mixed state, thus adding an electronic contribution to the electric field gradient in the nuclear region. This contribution could explain the higher values of the quadrupole interactions for the $3a$ sites. The possible presence of Fe^{4+} may be attributed to an electron transfer to the tantalum cations (i.e., $Ta^{5+} \rightarrow Ta^{4+}$) or, plausibly, due to some cation vacancies, in order to maintain the electronic neutrality of the compound.

Anyway, a comparison of the iron distributions between the $3a$ and $9e$ sites, for all R_2FeTaO_7, reveals, as a general trend, that the Rietveld analysis indicated a lower occupancy of iron for site $3e$ than the Mössbauer fits, as can be seen by inspecting of Tables I and II.

The Mössbauer spectra for the Gd_2FeTaO_7 and Y_2FeTaO_7 samples, obtained at 80 and 5 K, are shown in Fig. 4. There was no significant change in the Mössbauer patterns lowering the temperature down to 80 K (even in higher velocity measurements), the same occurring for Eu_2FeTaO_7 and Dy_2FeTaO_7 (spectra not shown). Thus, similar to the results obtained for the R_2FeSbO_7 series,[8,9] magnetic order is absent at 80 K for the iron sublattices. Apart from a small increase in the quadrupole splitting (QS), only an expected extra shift in the spectra due to the second-order Doppler effect can be verified.

However, for the sample measured at 5 K, a hyperfine magnetic splitting is present, revealing that some magnetic order has appeared at this temperature. The magnetic spectrum was fitted with a discrete sextet and a magnetic hyperfine field distribution. The angle θ, between the Z principal axis and the hyperfine magnetic field, was free to vary, whereas the QS was fixed with the same value of site $9e$ (chosen for reasons explained ahead) obtained at 80 K. The value of the hyperfine magnetic field thus obtained is of the same order of that previously reported for the R_2FeSbO_7 (R=Gd and Y) and $Y_2Fe_{1.33}W_{0.67}O_7$ pyrochlores (i.e., 40.0 and 43.0 T, respectively) (Refs. 8 and 11) although significantly smaller than our measurement for the Gd_2FeSbO_7 (i.e., 48.3 T).[6]

The well-defined sextet, unequivocally ascribable to only one site, indicated that one of the iron lattices turned out partially magnetic. Thus, a $3a$-$9e$ interaction strong enough

TABLE II. Hyperfine parameters and subspectral areas for the R_2FeTaO_7 compounds.

Pyrochlore	T (K)	Site/component	IS[a] (mm/s)	QS (mm/s)	B_{hf} (T)	Γ (mm/s)	Area (%)
Gd_2FeTaO_7	300	9*e*	0.31	0.71		0.29	59.3
		3*a*	0.20	1.77		0.26	40.7
	80	9*e*	0.39	0.74		0.32	54.3
		3*a*	0.28	1.87		0.28	45.7
	5	B_{hf} dist.	0.19	0.17	10.4[b]	0.30[c]	80.9
		Sextet	0.39	0.75[b]	40.6	0.25	19.1
			$\theta=63.5°$				
Eu_2FeTaO_7	300	9e	0.30	0.66		0.28	55.8
		3a	0.20	1.70		0.28	44.2
	80	9*e*	0.40	0.75		0.29	54.5
		3*a*	0.28	1.83		0.33	45.5
Dy_2FeTaO_7	300	9*e*	0.29	0.59		0.25	53.4
		3*a*	0.20	1.70		0.29	46.6
	80	9*e*	0.35	0.63		0.31	51.1
		3*a*	0.28	1.80		0.33	48.9
Y_2FeTaO_7	300	9*e*	0.30	0.67		0.33	56.8
		3*a*	0.21	1.79		0.33	43.2
	80	9*e*	0.35	0.67		0.35	53.8
		3*a*	0.23	1.81		0.34	46.2

[a]Relative to α-Fe.
[b]Average value.
[c]Fixed parameter.

to attribute some effective moment to iron in both sites may be discarded because it would give more than one Mössbauer sextet.

Therefore, only two magnetic interactions are possible in the present case: between the 9*e*-9*e* sites or the 3*a*-3*a* sites. The 3*a*-3*a* interaction, in particular, would need a double superexchange coupling of the Fe(3*a*)-O-Ta(9*e*)-O-Fe(3*a*) type, since a simple superexchange coupling is not allowed here (see Fig. 5). However, there are two angles, β_1's—both around 125° for the Gd_2FeTaO_7 at room temperature, to be considered in the double superexchange interaction for the site 3*a*, a situation not favored in this kind of coupling.[15] In addition, as far as we know, the literature does not report couplings between cations in octahedra and distorted square antiprism sites.

On the other hand, for the 9*e*-9*e* case a weak superexchange coupling 9*e*-O-9*e* could occur although again not by direct exchange because the distance between 9*e*-9*e* ions is too large (i.e., around 3.7 Å at RT for the Gd_2FeTaO_7 case). Considering that for iron oxides superexchange interaction at angles near to 90° gives antiferromagnetic couplings,[15,16] the 9*e* iron atoms would be atomic force microscopy oriented because their angles, β_2's, are close to 90° (Fig. 5).

In summary, the simplest model that could be realized is that of small islands of magnetically oriented 9*e* iron atoms (effectively, ~1/3 of them, according to MS), separated by tantalum atoms in the basal plane of the Gd_2FeTaO_7 crystallographic structure. Thus, frustration would be partially removed for the iron atoms of the 9*e* lattice, which would be magnetically oriented in a direction making $\theta+\xi$ with the *c* crystallographic axis. This could be in the direction of any of the straight lines that generate a cone, which axis practically lies in the basal plane, as shown in Fig. 6.

The temperature dependences of the inverse of susceptibility for the R_2FeTaO_7 samples are presented in Fig. 7. For comparison purposes, the curves for the $R_2Ti_2O_7$ (R=Eu and Gd) cubic pyrochlores are also shown. Two groups of curves are observed, one of them with gadolinium and dysprosium (i.e., cations with higher magnetic moment) and the other with europium and yttrium (cations with null or low magnetic moment).

It is worth mentioning that above 3 K the data obtained in field-cooled and zero-field-cooled modes coincide. These curves (not shown) were fitted with the Curie-Weiss expression, $\chi=C/(T-\Theta)$, where C and Θ are the Curie constant and

TABLE III. Data of the diagonal electric field gradients, calculated for both iron sites from the lattice contributions (i.e., using the refined atomic positions for the Gd_2FeTaO_7 compound).

Site ⇓	V_{ZZ} (arb. units)	η [a]	ζ
3*a*	0.70	0.48	97°, 5
9*e*	−0.49	0.78	91°, 3

[a]$\eta=(V_{XX}-V_{YY})/V_{ZZ}$ (asymmetry parameter).

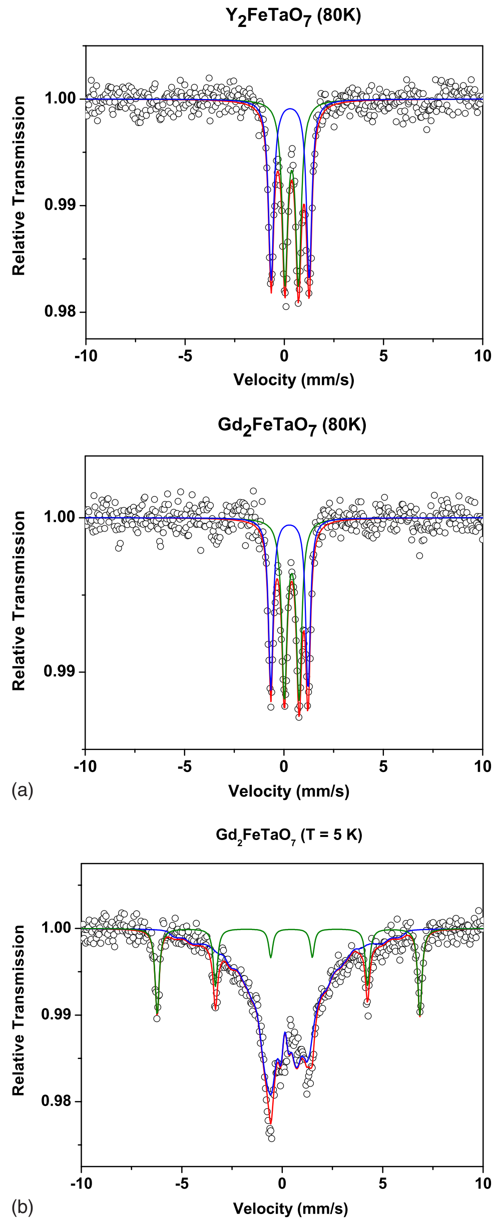

FIG. 4. (Color online) Low-temperature Mössbauer spectra for the Gd_2FeTaO_7 and Y_2FeTaO_7 samples: (a) 80 K and (b) 5 K.

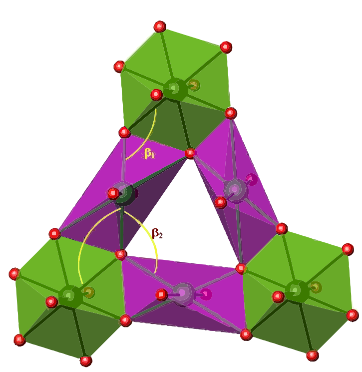

FIG. 5. (Color online) Triangular net of dodecahedra (in green) and octahedral (in violet) formed by the iron atoms—3*a* and 9*e*, respectively—and their neighbor oxygens, showing the angles between bonds. The red spheres are oxygen atoms.

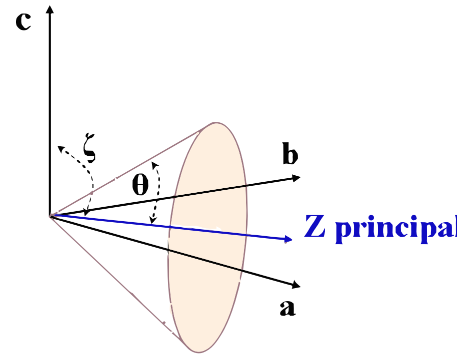

FIG. 6. (Color online) Conical surface where the magnetization direction lies for the Gd_2FeTaO_7 compound.

the paramagnetic Curie temperature, respectively. Values for the paramagnetic effective moment, μ_{eff}, were calculated from the Curie constants. Table IV shows the obtained parameters. It is observed that the $Eu_2Ti_2O_7$, Eu_2FeTaO_7, and Y_2FeTaO_7 compounds have large negative Θ values, an indication of strong antiferromagnetic correlations.

M versus *H* curves were also measured, at 2 K, and revealed that the magnetic moment does not saturate in fields up 9 T. However, a linear extrapolation of *M* versus $1/H$, to $1/H=0$, yields a lower estimate for the saturation moment, M_{sat}, also shown in the table. One sees that M_{sat} is much smaller then μ_{eff}, as expected for highly frustrated systems.

On the other hand, results for Gd_2FeTaO_7, $Gd_2Ti_2O_7$, and Dy_2FeTaO_7 show a larger effective magnetic moment, a direct consequence of the high moment of gadolinium and dysprosium. The parameters Θ are still negative but quite low, and the saturation moment is close to the effective moment, an indication that these compounds behave almost as standard paramagnets.

In any case, no clear magnetic phase transition could be verified, including for the Gd_2FeTaO_7 compound, in spite of the hyperfine magnetic field revealed by Mössbauer spectroscopy. Certainly, this can be attributed to the different time scales of both techniques.

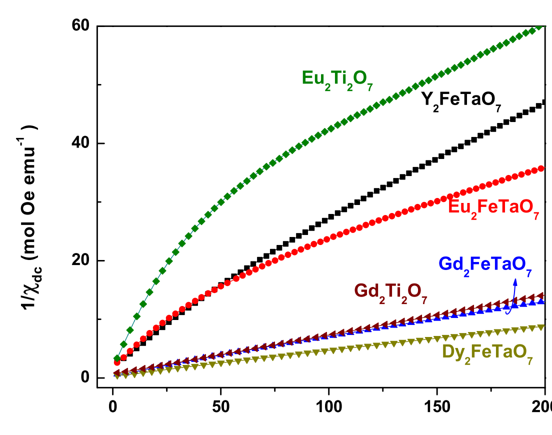

FIG. 7. (Color online) Temperature dependence of the inverse dc magnetic susceptibility, measured with $H=1$ T, for the R_2FeTaO_7 samples, together with some cubic pyrochlores.

TABLE IV. Magnetic data for the R_2FeTaO_7 compounds.

Pyrochlore	C (emu K/mol)	Θ (K)	μ_{eff} (μ_B)	M_{sat} [a] (μ_B)
$Eu_2Ti_2O_7$	5.55	−135	6.66	1.3
Eu_2FeTaO_7	9.28	−134	8.61	2.9
Y_2FeTaO_7	5.90	−81	6.87	2.2
Gd_2FeTaO_7	16.9	−21	11.6	13.9
$Gd_2Ti_2O_7$	14.6	−6.5	10.8	16.1
Dy_2FeTaO_7	24.0	−13	13.8	11.0

[a]Taken from the extrapolation of $1/H \rightarrow 0$ at $T=2$ K.

IV. CONCLUSIONS

The R_2FeTaO_7 pyrochlore-related compounds with R =Gd, Eu, Dy, and Y, crystallize with the **R3** symmetry and are paramagnetic at room temperature. Iron prefers the site $3a$ of the rhombohedral structure, where presents a $3+/4+$ mixed valence, for all R. There is no transition to long-range magnetic order down to 2 K although for the Gd_2FeTaO_7, at 5 K, an effective magnetic moment was observed for the $9e$ iron cation, indicating some starting short-range magnetic order.

ACKNOWLEDGMENTS

The authors would like to thank to CONICET and CNPq for the CIAM collaboration project. R.E.C. thanks ANPCYT (Project No. PICT 06-15102), CONICET (Project No. PIP 5767/05) and SECyT-UNC (Project No. 197/05). E.V.P.M. thanks CONICET. M.C.B. thanks ANPCYT.

[1] J. E. Greedan, J. Alloys Compd. **408-412**, 444 (2006).
[2] J. E. Greedan, J. Mater. Chem. **11**, 37 (2001).
[3] M. A. Subramanian, G. Aravamudan, and G. V. Subba Rao, Prog. Solid State Chem. **15**, 55 (1983).
[4] R. D. Shannon, Acta Crystallogr., Sect. A: Cryst. Phys., Diffr., Theor. Gen. Crystallogr. **32**, 751 (1976).
[5] A. F. Reid, C. Li, and A. E. Ringwood, J. Solid State Chem. **20**, 219 (1977).
[6] C. K. Matsuda, R. Barco, P. Sharma, V. Biondo, A. Paesano, Jr., J. B. M. Cunha, and B. Hallouche, Hyperfine Interact. **175**, 55 (2007).
[7] P. G. Casado, A. Mendiola, and I. Rasines, J. Phys. Chem. Solids **46**, 921 (1985).
[8] O. Knop, F. Brisse, R. E. Meads, and J. Bainbridge, Can. J. Chem. **46**, 3829 (1968).
[9] T. J. Snee, R. E. Meads, and W. G. Parker, J. Phys. C **10**, 1761 (1977).
[10] G. M. Veith, M. V. Lobanov, T. J. Emge, M. Greenblatt, M. Croft, F. Stowasser, J. Hadermann, and G. V. Tendeloo, J. Mater. Chem. **14**, 1623 (2004).
[11] G. Filoti, M. Rosenberg, V. Kuncser, B. Seling, T. Fries, A. Spies, and S. K. Sack, J. Alloys Compd. **268**, 16 (1998).
[12] J. Rodríguez-Carvajal, Physica B **192**, 55 (1993).
[13] *International Tables for Crystallography: Vol. A: Space Group Symmetry* (International Union of Crystallography, Heidelberg, 2006).
[14] V. I. Goldanskii and E. F. Makarov, in *Chemical Applications of Mössbauer Spectroscopy*, edited by V. I. Goldanskii and R. H. Herber (Academic, New York, 1968), Chap. 1.
[15] J. B. Goodenough, *Magnetism and the Chemical Bond* (Wiley InterScience, New York,1963).
[16] Y. Y. Li, Phys. Rev. **102**, 1015 (1956).